Ray tracing and geodesic deviation of the SH and SV reference rays in a heterogeneous generally anisotropic medium which is approximately transversely isotropic

Luděk Klimeš & Petr Bulant
Department of Geophysics, Faculty of Mathematics and Physics, Charles University in Prague, Ke Karlovu 3, 121 16 Praha 2, Czech Republic,
http://sw3d.cz/staff/klimes.htm, http://sw3d.cz/staff/bulant.htm

Summary

The coupling ray theory is usually applied to anisotropic common rays, but it is more accurate if it is applied to reference rays which are closer to the actual S–wave paths. If we know that a medium is close to transversely isotropic, it may be advantageous to trace reference rays which resemble the SH–wave and SV–wave rays. This paper is devoted to defining and tracing these SH and SV reference rays in a heterogeneous generally anisotropic medium which is approximately transversely isotropic, and to the corresponding equations of geodesic deviation (dynamic ray tracing).

The improvement of the coupling–ray–theory seismograms calculated along the proposed SH and SV reference rays, compared to the coupling–ray–theory seismograms calculated along the anisotropic common reference rays, is numerically demonstrated in two approximately transversely isotropic velocity models.

Keywords

Wave propagation, elastic anisotropy, heterogeneous media, S–wave coupling, transverse isotropy, symmetry axis, SH wave, SV wave, approximate transverse isotropy, reference symmetry axis, SH and SV reference rays.

1. Introduction

There may be a line intersection singularity at the slowness surface in a transversely isotropic medium. In this special case, the SH–wave and SV–wave rays smoothly cross this intersection singularity. However, this intersection singularity is unstable, and any perturbation from the transverse isotropy causes splitting of this intersection singularity (Crampin, 1981). The slower S–wave slowness sheet then separates from the faster S–wave slowness sheet, forming smooth but very sharp edges on both sheets (Bulant & Klimeš, 2014; Klimeš & Bulant, 2014b).

When the slowness vector of a ray smoothly passes through a split intersection singularity, the ray–velocity vector rapidly changes its direction and creates a sharp bend of the ray. This sharp bend is connected with a rapid rotation of the eigenvectors of the Christoffel matrix. The sharply bent rays thus cannot describe the correct wave propagation.

The actual S waves do not propagate along the sharply bent rays, but smoothly tunnel through a split intersection singularity (Klimeš & Bulant, 2012). If a medium

is close to transversely isotropic, the actual S–wave paths resemble the SH–wave and SV–wave rays.

The coupling ray theory (Chapman & Shearer, 1989; Bulant & Klimeš, 2002) is usually applied to anisotropic common rays (Bakker, 2002; Klimeš & Bulant, 2004; 2006; Klimeš, 2006; Bulant & Klimeš, 2008). On the other hand, the coupling ray theory is more accurate if it is applied to reference rays which are closer to the actual S–wave paths (Klimeš & Bulant, 2014a).

If we know that a medium is close to transversely isotropic, it is reasonable to trace reference rays which smoothly tunnel through a split intersection singularity and resemble the SH–wave and SV–wave rays. This paper is devoted to defining and tracing these SH and SV reference rays in a heterogeneous generally anisotropic medium which is approximately transversely isotropic, and to the corresponding equations of geodesic deviation (dynamic ray tracing).

Whether a medium is close to transversely isotropic can be determined by the method of Klimeš (2015). This method also determines the direction of the corresponding reference symmetry axis in terms of the reference symmetry vector.

In Section 5, we numerically demonstrate the improvement of the coupling–ray–theory seismograms calculated along the proposed SH and SV reference rays, compared to the coupling–ray–theory seismograms calculated along the anisotropic common reference rays, in approximately transversely isotropic velocity models SC1_I and SC1_II with a split intersection singularity by Pšenčík, Farra & Tessmer (2012). An analogous improvement in approximately transversely isotropic velocity models QI2 and QI4 without an intersection singularity was demonstrated previously by Klimeš & Bulant (2014a).

The lower–case Roman indices take values 1, 2 and 3. The upper–case Roman indices take values 1 and 2. Indices in parentheses are used to index the eigenvalues and eigenvectors of the Christoffel matrix. The Einstein summation over repetitive indices is used throughout the paper.

2. Reference SH and SV Hamiltonian functions

We assume that a given heterogeneous generally anisotropic medium is approximately transversely isotropic in directions perpendicular to given reference symmetry vector t_i. For the sake of simplicity, we consider the reference symmetry vector constant in this paper. However, the presented equations can simply be generalized to generally heterogeneous dependence of the reference symmetry vector on the spatial coordinates.

We project the reference symmetry vector onto the plane defined by two S–wave eigenvectors $g_{i(1)}$, $g_{i(2)}$ of the Christoffel matrix Γ_{jk}, and introduce the reference SV polarization in the direction of this projection. The unit reference SV polarization vector then reads

$$g_{i\mathrm{SV}} = \frac{g_{i(A)}\, g_{k(A)} t_k}{\sqrt{t_r g_{r(N)} g_{s(N)} t_s}} \quad . \tag{1}$$

We define *twice the reference SV Hamiltonian function* $G_{\mathrm{SV}} = 2\, H_{\mathrm{SV}}(x^m, p_n)$ homogeneous of the second degree with respect to slowness vector p_n as

$$G_{\mathrm{SV}} = g_{j\mathrm{SV}} \Gamma_{jk} g_{k\mathrm{SV}} \quad . \tag{2}$$

We then define *twice the reference SH Hamiltonian function* $G_{\mathrm{SH}} = 2\, H_{\mathrm{SH}}(x^m, p_n)$ homogeneous of the second degree with respect to slowness vector p_n in terms of twice

the reference SV Hamiltonian function as

$$G_{\mathrm{SH}} = G_{(1)} + G_{(2)} - G_{\mathrm{SV}} \quad , \tag{3}$$

where $G_{(1)}$ and $G_{(2)}$ are the S–wave eigenvalues of the Christoffel matrix.

As we need to handle both the derivatives with respect to spatial coordinates x^m and slowness–vector components p_n, we denote any partial phase–space derivative by $'$ or *.

The phase–space derivatives of twice the reference SH Hamiltonian function can then be expressed as

$$G'_{\mathrm{SH}} = G'_{(1)} + G'_{(2)} - G'_{\mathrm{SV}} \tag{4}$$

and

$$G'^{\star}_{\mathrm{SH}} = G'^{\star}_{(1)} + G'^{\star}_{(2)} - G'^{\star}_{\mathrm{SV}} \quad . \tag{5}$$

For the phase–space derivatives of the S–wave eigenvalues of the Christoffel matrix refer to Klimeš (2006. eqs. 22, 23). Hereinafter, we shall concentrate on the reference SV Hamiltonian function and its first–order and second–order phase–space derivatives.

We insert projection (1) into definition (2) and obtain

$$G_{\mathrm{SV}} = \frac{t_i g_{i(K)} g_{j(K)} \Gamma_{jk} g_{k(L)} g_{l(L)} t_l}{t_r g_{r(M)} g_{s(M)} t_s} \quad . \tag{6}$$

Since the eigenvectors of the Christoffel matrix are orthonormal,

$$g_{i(a)} g_{j(a)} = \delta_{ij} \quad , \tag{7}$$

we insert identity

$$g_{i(K)} g_{j(K)} = \delta_{ij} - g_{i(3)} g_{j(3)} \tag{8}$$

into expression (6), and obtain expression

$$G_{\mathrm{SV}} = \frac{t_i (\delta_{ij} - g_{i(3)} g_{j(3)}) \Gamma_{jk} (\delta_{kl} - g_{k(3)} g_{l(3)}) t_l}{t_r (\delta_{rs} - g_{r(3)} g_{s(3)}) t_s} \quad . \tag{9}$$

After multiplication, expression (9) reads

$$G_{\mathrm{SV}} = \frac{t_i \Gamma_{ij} t_j - (t_i g_{i(3)})^2 G_{(3)}}{t_s t_s - (t_s g_{s(3)})^2} \quad , \tag{10}$$

where

$$G_{(3)} = g_{i(3)} \Gamma_{ij} g_{j(3)} \tag{11}$$

is the P–wave eigenvalue of the Christoffel matrix. For simpler differentiation, we express relation (10) as

$$G_{\mathrm{SV}} = \frac{t_i \Gamma_{ij} t_j - G_{(3)} t_r t_r}{t_s t_s - (t_s g_{s(3)})^2} + G_{(3)} \quad . \tag{12}$$

3. Phase–space derivatives of the reference SV Hamiltonian function

3.1. Differentiating the reference SV Hamiltonian function

We now differentiate relation (12),

$$G'_{\mathrm{SV}} = \frac{t_i \Gamma'_{ij} t_j - G'_{(3)} t_r t_r}{t_s t_s - (t_s g_{s(3)})^2} + G'_{(3)} + 2 \frac{t_i \Gamma_{ij} t_j - G_{(3)} t_r t_r}{[t_s t_s - (t_s g_{s(3)})^2]^2} t_m g_{m(3)}\, t_n g'_{n(3)} \quad . \tag{13}$$

We again differentiate relation (13),

$$\begin{aligned} G'^{\star}_{\mathrm{SV}} = & \frac{t_i \Gamma'^{\star}_{ij} t_j - G'^{\star}_{(3)} t_r t_r}{t_s t_s - (t_s g_{s(3)})^2} + G'^{\star}_{(3)} + 2 \frac{t_i \Gamma'_{ij} t_j - G'_{(3)} t_r t_r}{[t_s t_s - (t_s g_{s(3)})^2]^2} t_m g_{m(3)}\, t_n g^{\star}_{n(3)} \\ & + 2 \frac{t_i \Gamma^{\star}_{ij} t_j - G^{\star}_{(3)} t_r t_r}{[t_s t_s - (t_s g_{s(3)})^2]^2} t_m g_{m(3)}\, t_n g'_{n(3)} + 8 \frac{t_i \Gamma_{ij} t_j - G_{(3)} t_r t_r}{[t_s t_s - (t_s g_{s(3)})^2]^3} \left(t_r g_{r(3)}\right)^2 t_m g'_{m(3)}\, t_n g^{\star}_{n(3)} \\ & + 2 \frac{t_i \Gamma_{ij} t_j - G_{(3)} t_r t_r}{[t_s t_s - (t_s g_{s(3)})^2]^2} \left(t_m g'_{m(3)}\, t_n g^{\star}_{n(3)} + t_m g_{m(3)}\, t_n g'^{\star}_{n(3)} \right) \quad . \end{aligned} \tag{14}$$

We insert relation (12) and identity

$$t_s t_s - (t_s g_{s(3)})^2 = t_r g_{r(M)} g_{s(M)} t_s \tag{15}$$

into relation (13),

$$G'_{\mathrm{SV}} = \frac{t_i \Gamma'_{ij} t_j - G'_{(3)} t_r t_r}{t_r g_{r(M)} g_{s(M)} t_s} + G'_{(3)} - 2 \frac{G_{(3)} - G_{\mathrm{SV}}}{t_r g_{r(M)} g_{s(M)} t_s} t_m g_{m(3)}\, t_n g'_{n(3)} \quad , \tag{16}$$

and into relation (14),

$$\begin{aligned} G'^{\star}_{\mathrm{SV}} = & \frac{t_i \Gamma'^{\star}_{ij} t_j - G'^{\star}_{(3)} t_r t_r}{t_r g_{r(M)} g_{s(M)} t_s} + G'^{\star}_{(3)} + 2 \frac{t_i \Gamma'_{ij} t_j - G'_{(3)} t_r t_r}{(t_r g_{r(M)} g_{s(M)} t_s)^2} t_m g_{m(3)}\, t_n g^{\star}_{n(3)} \\ & + 2 \frac{t_i \Gamma^{\star}_{ij} t_j - G^{\star}_{(3)} t_r t_r}{(t_r g_{r(M)} g_{s(M)} t_s)^2} t_m g_{m(3)}\, t_n g'_{n(3)} - 8 \frac{G_{(3)} - G_{\mathrm{SV}}}{(t_r g_{r(M)} g_{s(M)} t_s)^2} \left(t_r g_{r(3)}\right)^2 t_m g'_{m(3)}\, t_n g^{\star}_{n(3)} \\ & - 2 \frac{G_{(3)} - G_{\mathrm{SV}}}{t_r g_{r(M)} g_{s(M)} t_s} \left(t_m g'_{m(3)}\, t_n g^{\star}_{n(3)} + t_m g_{m(3)}\, t_n g'^{\star}_{n(3)} \right) \quad . \end{aligned} \tag{17}$$

3.2. Transformation into the eigenvectors of the Christoffel matrix

We define the elements of the Christoffel matrix and of its phase–space derivatives with respect to the eigenvectors of the Christoffel matrix as

$$\Gamma_{(ab)} = g_{i(a)} \Gamma_{ij}\, g_{j(b)} \quad , \tag{18}$$

$$\Gamma'_{(ab)} = g_{i(a)} \Gamma'_{ij}\, g_{j(b)} \tag{19}$$

and

$$\Gamma'^{\star}_{(ab)} = g_{i(a)} \Gamma'^{\star}_{ij}\, g_{j(b)} \quad . \tag{20}$$

Note that $\Gamma_{(ab)}$ is a diagonal matrix with diagonal elements

$$\Gamma_{(aa)} = G_{(a)} \quad , \tag{21}$$

and that the first–order phase–space derivatives of the eigenvalues of the Christoffel matrix represent the diagonal elements of symmetric matrix $\Gamma'_{(ab)}$ (Klimeš, 2006. eq. 22),

$$G'_{(a)} = \Gamma'_{(aa)} \quad . \tag{22}$$

We define the components

$$t_{(a)} = t_n \, g_{n(a)} \tag{23}$$

of reference symmetry vector t_i with respect to the eigenvectors of the Christoffel matrix.

We insert definitions (18) and (23) into definition (6) and obtain relation

$$G_{\rm SV} = \frac{t_{(A)} \Gamma_{(AB)} t_{(B)}}{t_{(S)} t_{(S)}} \quad , \tag{24}$$

which can be expressed considering (21) as

$$\boxed{G_{\rm SV} = \frac{\sum_A G_{(A)} (t_{(A)})^2}{t_{(S)} t_{(S)}} \quad .} \tag{25}$$

We insert definitions (19) and (23) and relation (22) into relation (16), and obtain

$$G'_{\rm SV} = \frac{t_{(a)} \Gamma'_{(ab)} t_{(b)} - (t_{(3)})^2 \Gamma'_{(33)}}{t_{(S)} t_{(S)}} - 2 \frac{G_{(3)} - G_{\rm SV}}{t_{(S)} t_{(S)}} t_{(3)} \, t_n g'_{n(3)} \tag{26}$$

We insert definitions (19), (20) and (23) and relation (22) into relation (17), and arrive at

$$\begin{aligned} G'^{\star}_{\rm SV} = & \frac{t_{(a)} \Gamma'^{\star}_{(ab)} t_{(b)} - (t_{(3)})^2 \Gamma'^{\star}_{(33)}}{t_{(S)} t_{(S)}} + 2 \frac{t_{(a)} \Gamma'_{(ab)} t_{(b)} - \Gamma'_{(33)} t_{(r)} t_{(r)}}{(t_{(S)} t_{(S)})^2} t_{(3)} \, t_n g^{\star}_{n(3)} \\ & + 2 \frac{t_{(a)} \Gamma^{\star}_{(ab)} t_{(b)} - \Gamma^{\star}_{(33)} t_{(r)} t_{(r)}}{(t_{(S)} t_{(S)})^2} t_{(3)} \, t_n g'_{n(3)} - 8 \frac{G_{(3)} - G_{\rm SV}}{(t_{(S)} t_{(S)})^2} \left(t_{(3)}\right)^2 t_m g'_{m(3)} \, t_n g^{\star}_{n(3)} \\ & - 2 \frac{G_{(3)} - G_{\rm SV}}{t_{(S)} t_{(S)}} \left(t_m g'_{m(3)} \, t_n g^{\star}_{n(3)} + t_{(3)} \, t_n g'^{\star}_{n(3)} \right) \quad , \end{aligned} \tag{27}$$

which can be expressed as

$$\begin{aligned} G'^{\star}_{\rm SV} = & \frac{t_{(a)} \Gamma'^{\star}_{(ab)} t_{(b)} - (t_{(3)})^2 G'^{\star}_{(3)}}{t_{(S)} t_{(S)}} + 2 \frac{t_{(a)} \Gamma'_{(ab)} t_{(b)} - \Gamma'_{(33)} t_{(r)} t_{(r)}}{(t_{(S)} t_{(S)})^2} t_{(3)} \, t_n g^{\star}_{n(3)} \\ & + 2 \frac{t_{(a)} \Gamma^{\star}_{(ab)} t_{(b)} - \Gamma^{\star}_{(33)} t_{(r)} t_{(r)}}{(t_{(S)} t_{(S)})^2} t_{(3)} \, t_n g'_{n(3)} - 2 \frac{G_{(3)} - G_{\rm SV}}{t_{(S)} t_{(S)}} \left(1 + 4 \, \frac{(t_{(3)})^2}{t_{(S)} t_{(S)}} \right) t_m g'_{m(3)} \, t_n g^{\star}_{n(3)} \\ & - 2 \frac{G_{(3)} - G_{\rm SV}}{t_{(S)} t_{(S)}} t_{(3)} \, t_n g'^{\star}_{n(3)} \quad . \end{aligned} \tag{28}$$

We now have to express the second–order phase–space derivatives of the eigenvalues of the Christoffel matrix and the first–order and second–order phase–space derivatives of the eigenvectors of the Christoffel matrix in relations (26) and (28) in terms of the phase–space derivatives of the Christoffel matrix.

3.3. Second–order phase–space derivatives of the eigenvalues of the Christoffel matrix

The expression for the second–order phase–space derivatives of the eigenvalues of the Christoffel matrix is (Klimeš, 2006. eq. 23)

$$G'^{\star}_{(a)} = \Gamma'^{\star}_{(aa)} + 2 \sum_{b \neq a} \frac{\Gamma'_{(ab)} \Gamma^{\star}_{(ab)}}{G_{(a)} - G_{(b)}} \quad , \tag{29}$$

which for $a = 3$ reads

$$G'^{\star}_{(3)} = \Gamma'^{\star}_{(33)} + 2\sum_{B} \frac{\Gamma'_{(B3)}\Gamma^{\star}_{(B3)}}{G_{(3)} - G_{(B)}} \quad . \tag{30}$$

This expression can be inserted into relation (28).

3.4. First–order phase–space derivatives of the eigenvectors of the Christoffel matrix

The first–order phase–space derivatives of the eigenvectors of the Christoffel matrix can be expressed as (Klimeš, 2006. eq. 17)

$$g'_{i(a)} = \sum_{b \neq a} g_{i(b)} \frac{g_{j(b)}\Gamma'_{jk}g_{k(a)}}{G_{(a)} - G_{(b)}} \quad , \tag{31}$$

which for $a = 3$ with definition (19) reads

$$g'_{i(3)} = \sum_{B} g_{i(B)} \frac{\Gamma'_{(B3)}}{G_{(3)} - G_{(B)}} \quad . \tag{32}$$

We multiply relation (32) by reference symmetry vector t_i and obtain expression

$$t_n g'_{n(3)} = \sum_{A} t_{(A)} \frac{\Gamma'_{(A3)}}{G_{(3)} - G_{(A)}} \tag{33}$$

which can be inserted into relations (26) and (28).

3.5. Second–order phase–space derivatives of the eigenvectors of the Christoffel matrix

The second–order phase–space derivatives of the eigenvectors of the Christoffel matrix can be obtained by twice differentiating the Christoffel equation (Klimeš, 2006. eq. 11),

$$g'^{\star}_{i(a)}G_{(a)} + g'_{i(a)}G^{\star}_{(a)} + g^{\star}_{i(a)}G'_{(a)} + g_{i(a)}G'^{\star}_{(a)} = \Gamma'^{\star}_{ij}g_{j(a)} + \Gamma'_{ij}g^{\star}_{j(a)} + \Gamma^{\star}_{ij}g'_{j(a)} + \Gamma_{ij}g'^{\star}_{j(a)} \quad . \tag{34}$$

We multiply relation (34) for $a = 3$ by eigenvector $g_{i(C)}$ of the Christoffel matrix,

$$g_{i(C)}g'^{\star}_{i(3)}G_{(3)} + g_{i(C)}g'_{i(3)}G^{\star}_{(3)} + g_{i(C)}g^{\star}_{i(3)}G'_{(3)} = g_{i(C)}\Gamma'^{\star}_{ij}g_{j(3)} + g_{i(C)}\Gamma'_{ij}g^{\star}_{j(3)} + g_{i(C)}\Gamma^{\star}_{ij}g'_{j(3)} + g_{i(C)}\Gamma_{ij}g'^{\star}_{j(3)} . \tag{35}$$

We then express two components of the second–order phase–space derivatives of the eigenvector of the Christoffel matrix as

$$g_{i(C)}g'^{\star}_{i(3)} = \frac{g_{i(C)}\Gamma'^{\star}_{ij}g_{j(3)} + g_{i(C)}\Gamma'_{ij}g^{\star}_{j(3)} + g_{i(C)}\Gamma^{\star}_{ij}g'_{j(3)} - g_{i(C)}g'_{i(3)}G^{\star}_{(3)} - g_{i(C)}g^{\star}_{i(3)}G'_{(3)}}{G_{(3)} - G_{(C)}} \quad . \tag{36}$$

Since the eigenvectors of the Christoffel matrix are unit, the third component of the second–order phase–space derivatives of the eigenvector of the Christoffel matrix can be expressed in terms of its first–order phase–space derivatives as

$$g_{i(3)}g'^{\star}_{i(3)} = -g'_{i(3)}g^{\star}_{i(3)} \quad . \tag{37}$$

We insert relations (22) and (32) into expression (36) and obtain

$$g_{i(C)}g'^{\star}_{i(3)} = \frac{g_{i(C)}\Gamma'^{\star}_{ij}g_{j(3)}}{G_{(3)} - G_{(C)}} + \sum_{B} \frac{g_{i(C)}\Gamma'_{ij}g_{j(B)}\Gamma^{\star}_{(B3)} + g_{i(C)}\Gamma^{\star}_{ij}g_{j(B)}\Gamma'_{(B3)}}{(G_{(3)} - G_{(C)})(G_{(3)} - G_{(B)})} - \sum_{B} \frac{g_{i(C)}g_{i(B)}\Gamma'_{(B3)}\Gamma^{\star}_{(33)} + g_{i(C)}g_{i(B)}\Gamma^{\star}_{(B3)}\Gamma'_{(33)}}{(G_{(3)} - G_{(C)})(G_{(3)} - G_{(B)})} \quad , \tag{38}$$

which with definitions (19) and (20) reads

$$g_{i(C)}\,g'^{\star}_{i(3)} = \frac{\Gamma'^{\star}_{(C3)}}{G_{(3)}-G_{(C)}} + \sum_{B}\frac{\Gamma'_{(CB)}\Gamma^{\star}_{(B3)}+\Gamma^{\star}_{(CB)}\Gamma'_{(B3)}}{(G_{(3)}-G_{(C)})(G_{(3)}-G_{(B)})} - \frac{\Gamma'_{(C3)}\Gamma^{\star}_{(33)}+\Gamma^{\star}_{(C3)}\Gamma'_{(33)}}{(G_{(3)}-G_{(C)})^2} \quad . \tag{39}$$

We insert relation (32) into identity (37) and obtain

$$g_{i(3)}\,g'^{\star}_{i(3)} = -\sum_{C}\frac{\Gamma'_{(C3)}\Gamma^{\star}_{(C3)}}{(G_{(3)}-G_{(C)})^2} \quad . \tag{40}$$

Relations (39) and (40) yield expression

$$\begin{aligned} t_n\,g'^{\star}_{n(3)} = &\sum_{C} t_{(C)}\frac{\Gamma'^{\star}_{(C3)}}{G_{(3)}-G_{(C)}} + \sum_{C} t_{(C)}\sum_{B}\frac{\Gamma'_{(CB)}\Gamma^{\star}_{(B3)}+\Gamma^{\star}_{(CB)}\Gamma'_{(B3)}}{(G_{(3)}-G_{(C)})(G_{(3)}-G_{(B)})} \\ &- \sum_{C} t_{(C)}\frac{\Gamma'_{(C3)}\Gamma^{\star}_{(33)}+\Gamma^{\star}_{(C3)}\Gamma'_{(33)}}{(G_{(3)}-G_{(C)})^2} - t_{(3)}\sum_{C}\frac{\Gamma'_{(C3)}\Gamma^{\star}_{(C3)}}{(G_{(3)}-G_{(C)})^2} \end{aligned} \tag{41}$$

which can be inserted into relation (28).

3.6. First–order and second–order phase–space derivatives of the reference SV Hamiltonian function

We insert expression (33) into relation (26),

$$G'_{\mathrm{SV}} = \frac{t_{(a)}\Gamma'_{(ab)}t_{(b)}-(t_{(3)})^2\Gamma'_{(33)}}{t_{(S)}t_{(S)}} - 2\frac{G_{(3)}-G_{\mathrm{SV}}}{t_{(S)}t_{(S)}}t_{(3)}\sum_{N} t_{(N)}\frac{\Gamma'_{(N3)}}{G_{(3)}-G_{(N)}} \quad . \tag{42}$$

We insert expressions (30), (33) and (41) into relation (28), and obtain

$$\begin{aligned} G'^{\star}_{\mathrm{SV}} = &\frac{t_{(a)}\Gamma'^{\star}_{(ab)}t_{(b)}-(t_{(3)})^2\Gamma'^{\star}_{(33)}}{t_{(S)}t_{(S)}} - \frac{2\,(t_{(3)})^2}{t_{(S)}t_{(S)}}\sum_{B}\frac{\Gamma'_{(B3)}\Gamma^{\star}_{(B3)}}{G_{(3)}-G_{(B)}} \\ &+ 2\frac{t_{(a)}\Gamma'_{(ab)}t_{(b)}-\Gamma'_{(33)}t_{(r)}t_{(r)}}{(t_{(S)}t_{(S)})^2}t_{(3)}\sum_{N} t_{(N)}\frac{\Gamma^{\star}_{(N3)}}{G_{(3)}-G_{(N)}} \\ &+ 2\frac{t_{(a)}\Gamma^{\star}_{(ab)}t_{(b)}-\Gamma^{\star}_{(33)}t_{(r)}t_{(r)}}{(t_{(S)}t_{(S)})^2}t_{(3)}\sum_{N} t_{(N)}\frac{\Gamma'_{(N3)}}{G_{(3)}-G_{(N)}} \\ &- 2\frac{G_{(3)}-G_{\mathrm{SV}}}{t_{(S)}t_{(S)}}\left(1+4\,\frac{(t_{(3)})^2}{t_{(S)}t_{(S)}}\right)\left(\sum_{M} t_{(M)}\frac{\Gamma'_{(M3)}}{G_{(3)}-G_{(M)}}\right)\left(\sum_{N} t_{(N)}\frac{\Gamma^{\star}_{N3}}{G_{(3)}-G_{(N)}}\right) \\ &- 2\frac{G_{(3)}-G_{\mathrm{SV}}}{t_{(S)}t_{(S)}}t_{(3)}\sum_{C}\left(t_{(C)}\frac{\Gamma'^{\star}_{(C3)}}{G_{(3)}-G_{(C)}} + t_{(C)}\sum_{B}\frac{\Gamma'_{(CB)}\Gamma^{\star}_{(B3)}+\Gamma^{\star}_{(CB)}\Gamma'_{(B3)}}{(G_{(3)}-G_{(C)})(G_{(3)}-G_{(B)})}\right. \\ &\left. - t_{(C)}\frac{\Gamma'_{(C3)}\Gamma^{\star}_{(33)}+\Gamma^{\star}_{(C3)}\Gamma'_{(33)}}{(G_{(3)}-G_{(C)})^2} - t_{(3)}\frac{\Gamma'_{(C3)}\Gamma^{\star}_{(C3)}}{(G_{(3)}-G_{(C)})^2}\right) \quad . \end{aligned} \tag{43}$$

The colours in relation (43) will serve for referencing individual terms of the relation in the next section.

4. Weighting factors of the phase–space derivatives of the Christoffel matrix

4.1. Reference SV Hamiltonian function

We express the first–order phase–space derivatives of twice the reference SV Hamiltonian function G_{SV} in terms of the first–order phase–space derivatives of the Christoffel matrix,

$$G'_{\mathrm{SV}} = \sum_a \sum_b w'_{(ab)} \Gamma'_{(ab)} \quad . \tag{44}$$

The weighting factors in expression (44) obey symmetry relation

$$w'_{(ab)} = w'_{(ba)} \quad . \tag{45}$$

We express the second–order phase–space derivatives of G_{SV} in terms of the first–order and second–order phase–space derivatives of the Christoffel matrix,

$$G'^{\star}_{\mathrm{SV}} = \sum_a \sum_b w'^{\star}_{(ab)} \Gamma'^{\star}_{(ab)} + \sum_a \sum_b \sum_c \sum_d w'^{\star}_{(abcd)} \Gamma'_{(ab)} \Gamma^{\star}_{(cd)} \quad . \tag{46}$$

The weighting factors in expression (46) obey symmetry relations

$$w'^{\star}_{(ab)} = w'^{\star}_{(ba)} \tag{47}$$

and

$$w'^{\star}_{(abcd)} = w'^{\star}_{(bacd)} = w'^{\star}_{(abdc)} = w'^{\star}_{(cdab)} \quad . \tag{48}$$

The weighting factors in expression (44) can be obtained from relation (42) as

$$w'_{(AB)} = \frac{t_{(A)} t_{(B)}}{t_{(S)} t_{(S)}} \quad , \tag{49}$$

$$w'_{(A3)} = \frac{t_{(A)} t_{(3)}}{t_{(S)} t_{(S)}} - \frac{G_{(3)} - G_{\mathrm{SV}}}{t_{(S)} t_{(S)}} \frac{t_{(A)} t_{(3)}}{G_{(3)} - G_{(A)}} \quad , \tag{50}$$

which can be expressed as

$$w'_{(A3)} = \frac{t_{(A)} t_{(3)}}{t_{(S)} t_{(S)}} \frac{G_{\mathrm{SV}} - G_{(A)}}{G_{(3)} - G_{(A)}} \quad , \tag{51}$$

and

$$w'_{(33)} = 0 \quad . \tag{52}$$

Note that the weighting factors are independent of particular phase–space derivatives $'$.

The weighting factors in expression (46) can be obtained from relation (43), and are again independent of particular phase–space derivatives $'$ and $\star$. The terms with blue in relation (43) correspond to weighting factors

$$w'^{\star}_{(AB)} = w'_{(AB)} \quad , \tag{53}$$

$$w'^{\star}_{(A3)} = w'_{(A3)} \quad , \tag{54}$$

$$w'^{\star}_{(33)} = 0 \quad . \tag{55}$$

There are no terms in relation (43) corresponding to weighting factors

$$w'^{\star}_{(ABCD)} = 0 \quad , \tag{56}$$

$$w'^{\star}_{(AB33)} = 0 \quad , \tag{57}$$

$$w'^{\star}_{(3333)} = 0 \quad . \tag{58}$$

The second and third lines and the first term with green in relation (43) yield weighting factors

$$w'^{\star}_{(ABC3)} = \frac{t_{(A)}t_{(B)}t_{(C)}t_{(3)}}{(G_{(3)}-G_{(C)})\,(t_{(S)}t_{(S)})^2} - \frac{(G_{(3)}-G_{\mathrm{SV}})\,(t_{(A)}\delta_{BC}+t_{(B)}\delta_{AC})\,t_{(3)}}{2\,(G_{(3)}-G_{(A)})\,(G_{(3)}-G_{(B)})\,t_{(S)}t_{(S)}} \quad . \tag{59}$$

The second and third lines and the terms with red in relation (43) yield weighting factors

$$\begin{aligned} w'^{\star}_{(A3C3)} = {} & \frac{t_{(A)}t_{(3)}t_{(C)}t_{(3)}}{(t_{(S)}t_{(S)})^2}\left(\frac{1}{G_{(3)}-G_{(A)}}+\frac{1}{G_{(3)}-G_{(C)}}\right) - \frac{\delta_{AC}(t_{(3)})^2}{2\,t_{(S)}t_{(S)}\,(G_{(3)}-G_{(A)})} \\ & - \frac{G_{(3)}-G_{\mathrm{SV}}}{2\,(G_{(3)}-G_{(A)})(G_{(3)}-G_{(C)})}\left[\frac{t_{(A)}t_{(C)}}{t_{(S)}t_{(S)}}\left(1+4\,\frac{(t_{(3)})^2}{t_{(R)}t_{(R)}}\right)-\delta_{AC}\frac{(t_{(3)})^2}{t_{(S)}t_{(S)}}\right] \quad . \end{aligned} \tag{60}$$

The second and third lines and the second term with green in relation (43) yield weighting factors

$$w'^{\star}_{(A333)} = -\frac{t_{(A)}t_{(3)}}{t_{(S)}t_{(S)}\,(G_{(3)}-G_{(A)})} + \frac{G_{(3)}-G_{\mathrm{SV}}}{t_{(S)}t_{(S)}}\frac{t_{(A)}t_{(3)}}{(G_{(3)}-G_{(A)})^2} \quad . \tag{61}$$

Relation (60) can be expressed as

$$\begin{aligned} w'^{\star}_{(A3C3)} = {} & \frac{1}{G_{(3)}-G_{(A)}}\;\frac{1}{G_{(3)}-G_{(C)}} \\ & \times\left\{\left[\frac{G_{(3)}-G_{(A)}}{2}+\frac{G_{(3)}-G_{(C)}}{2}\right]\left[2\,\frac{t_{(A)}t_{(3)}t_{(C)}t_{(3)}}{(t_{(S)}t_{(S)})^2}-\frac{\delta_{AC}}{2}\frac{(t_{(3)})^2}{t_{(S)}t_{(S)}}\right]\right. \\ & \left.-\left(G_{(3)}-G_{\mathrm{SV}}\right)\left[\frac{t_{(A)}t_{(C)}}{t_{(S)}t_{(S)}}\left(\frac{1}{2}+2\,\frac{(t_{(3)})^2}{t_{(R)}t_{(R)}}\right)-\frac{\delta_{AC}}{2}\frac{(t_{(3)})^2}{t_{(S)}t_{(S)}}\right]\right\} \quad , \end{aligned} \tag{62}$$

and finally as

$$\begin{aligned} w'^{\star}_{(A3C3)} = {} & \frac{1}{G_{(3)}-G_{(A)}}\;\frac{1}{G_{(3)}-G_{(C)}} \\ & \times\left[\left(G_{\mathrm{SV}}-\frac{G_{(A)}}{2}-\frac{G_{(C)}}{2}\right)\frac{(t_{(3)})^2}{t_{(R)}t_{(R)}}\left(2\,\frac{t_{(A)}t_{(C)}}{t_{(S)}t_{(S)}}-\frac{\delta_{AC}}{2}\right)-\frac{G_{(3)}-G_{\mathrm{SV}}}{2}\;\frac{t_{(A)}t_{(C)}}{t_{(S)}t_{(S)}}\right] \quad . \end{aligned} \tag{63}$$

Relation (61) can be expressed as

$$w'^{\star}_{(A333)} = -\frac{t_{(A)}t_{(3)}}{t_{(R)}t_{(R)}}\;\frac{G_{\mathrm{SV}}-G_{(A)}}{(G_{(3)}-G_{(A)})^2} \quad , \tag{64}$$

and finally as

$$w'^{\star}_{(A333)} = -\frac{w'_{(A3)}}{G_{(3)}-G_{(A)}} \quad . \tag{65}$$

4.2. Reference SH Hamiltonian function

We express the first–order phase–space derivatives of twice the reference SH Hamiltonian function G_{SH} in terms of the first–order phase–space derivatives of the Christoffel matrix,

$$G'_{\mathrm{SH}} = \sum_a \sum_b \widetilde{w}'_{(ab)} \Gamma'_{(ab)} \quad . \tag{66}$$

The weighting factors in expression (66) obey symmetry relation (45) analogously as the weighting factors in expression (44).

We express the second–order phase–space derivatives of G_{SH} in terms of the first–order and second–order phase–space derivatives of the Christoffel matrix,

$$G'^{\star}_{\mathrm{SH}} = \sum_a \sum_b \widetilde{w}'^{\star}_{(ab)} \Gamma'^{\star}_{(ab)} + \sum_a \sum_b \sum_c \sum_d \widetilde{w}'^{\star}_{(abcd)} \Gamma'_{(ab)} \Gamma^{\star}_{(cd)} \quad . \tag{67}$$

The weighting factors in expression (67) obey symmetry relations (47) and (48) analogously as the weighting factors in expression (46).

Relations (4), (5), (22), (29) and (53)–(55) yield weighting factors

$$\widetilde{w}'^{\star}_{(11)} = \widetilde{w}'_{(11)} = 1 - w'_{(11)} \quad , \tag{68}$$

$$\widetilde{w}'^{\star}_{(22)} = \widetilde{w}'_{(22)} = 1 - w'_{(22)} \quad , \tag{69}$$

$$\widetilde{w}'^{\star}_{(1313)} = -\frac{1}{2\,(G_{(3)} - G_{(1)})} - w'^{\star}_{(1313)} \quad , \tag{70}$$

$$\widetilde{w}'^{\star}_{(2323)} = -\frac{1}{2\,(G_{(3)} - G_{(2)})} - w'^{\star}_{(2323)} \quad . \tag{71}$$

All other weighting factors in expressions (66) and (67) are

$$\widetilde{w}'^{\star}_{(ab)} = \widetilde{w}'_{(ab)} = -w'_{(ab)} \quad , \tag{72}$$

$$\widetilde{w}'^{\star}_{(abcd)} = -w'^{\star}_{(abcd)} \quad . \tag{73}$$

5. Numerical examples

The above described algorithm of calculating the the first–order and second–order phase–space derivatives of the reference SH and SV Hamiltonian functions has been coded as a new option of subroutine file `hder.for` of software package MODEL (Bucha & Bulant, 2015). Tracing the SH and SV reference rays in smoothly heterogeneous generally anisotropic velocity models which are approximately transversely isotropic with respect to a constant reference symmetry vector can thus be used as a new option of ray tracing program `crt.for` of software package CRT (Bucha & Bulant, 2015).

The algorithm for sorting the SH and SV reference rays according to Klimeš & Bulant (2014a, sec. 4.1) has been coded as a new program `greenti.for` of software package CRT (Bucha & Bulant, 2015). Note that this program is not applicable to velocity models QIH, QI, QI2 and QI4 (Klimeš & Bulant, 2012) because of too great rotation of the eigenvectors of the Christoffel matrix. In these velocity models we use sorting according to Klimeš & Bulant (2014a, sec. 4.2).

Bulant et al. (2011) and Klimeš & Bulant (2012) compared the coupling ray theory for S waves and its prevailing–frequency approximation with the *Fourier pseudospectral method* (Pšenčík, Farra & Tessmer, 2012) which was considered as a nearly exact reference. The coupling–ray–theory seismograms were calculated along the anisotropic common S–wave reference rays with the second–order perturbation expansion of S–wave travel times. The comparison was performed in seven velocity models: six velocity models QI, QI2, QI4, KISS, SC1_I and SC1_II are approximately transversely isotropic, velocity model ORT is orthorhombic. These anisotropic velocity models with related input data can be found in package DATA (Bucha & Bulant, 2015).

The coupling–ray–theory seismograms in approximately transversely isotropic velocity models QI and KISS were nearly equal to the Fourier pseudospectral method (Klimeš & Bulant, 2012, figs. 3, 8). The coupling–ray–theory seismograms in orthorhombic velocity model ORT differed from the Fourier pseudospectral method approximately by the thickness of line (Klimeš & Bulant, 2012, fig. 9).

Approximately transversely isotropic velocity models QI2 and QI4 contain no intersection singularity. In this case, the SH and SV reference rays correspond to the faster and slower anisotropic–ray–theory S waves. This property was exploited by Klimeš & Bulant (2014a), who calculated the coupling–ray–theory seismograms in velocity models QI2 and QI4 along the SH and SV reference rays and demonstrated their substantial improvement and agreement with the Fourier pseudospectral method.

Hereinafter, we shall present the coupling–ray–theory seismograms calculated in remaining two approximately transversely isotropic velocity models SC1_I and SC1_II along the SH and SV reference rays proposed in this paper. In velocity model SC1_II containing a split intersection singularity, Klimeš & Bulant (2012, fig. 7) observed the greatest inaccuracy of the coupling–ray–theory seismograms calculated along the anisotropic common S–wave reference rays. Bulant & Klimeš (2014) and Klimeš & Bulant (2014b) then demonstrated that the anisotropic–ray–theory reference rays are not applicable in velocity model SC1_II, which lead to the proposal of tracing the SH and SV reference rays in generally anisotropic velocity models which are approximately transversely isotropic.

5.1. Anisotropic velocity models

We consider here two approximately transversely isotropic velocity models SC1_I and SC1_II. Both these velocity models are laterally homogeneous. The density is constant. The elastic moduli are linear functions of depth.

At the depth of 0 km, velocity model SC1_I is approximately transversely isotropic and its axis of symmetry is horizontal. At this depth, the slowness surface contains an intersection singularity, whereas velocity models QIH, QI, QI2 and QI4 display no intersection singularity (Pšenčík, Farra & Tessmer, 2012). At the depth of 1.5 km, velocity model SC1_I is very close to isotropic, but is slightly cubic and its symmetry axes coincide with the coordinate axes. This means that, at depths between 0 km and 1.5 km, velocity model SC1_I is very close to transversely isotropic, but is slightly tetragonal. Whereas the transversely isotropic medium contains the intersection singularity through which the rays pass without rotation of the eigenvectors of the Christoffel matrix (Vavryčuk, 2001, sec. 4.3; Klimeš & Bulant, 2014a), in the approximately transversely isotropic medium, the S–wave slowness surface is split at this unstable singularity (Crampin, 1981) and the eigenvectors of the Christoffel matrix rapidly rotate by 90° there. This split intersection singularity then acts as an interface and smoothly but very rapidly converts the actual S–wave polarizations from the approximately anisotropic–ray–theory polarization S1 to the approximately anisotropic–ray–theory polarization S2, and vice versa.

Velocity model SC1_II is analogous to SC1_I, but the axis of symmetry of its transversely isotropic component is tilted, refer to Pšenčík, Farra & Tessmer (2012). The symmetry axes of its weak cubic component coincide with the coordinate axes. The split intersection singularity in velocity model SC1_II is thus positioned differently in comparison with velocity model SC1_I. In the source–receiver plane, the split intersection singularity is close to horizontal slowness vectors. The deviation of the anisotropic–ray–theory rays from both the anisotropic common reference rays and the actual wave paths is much greater in velocity model SC1_II than in velocity model SC1_I (Pšenčík, Farra & Tessmer, 2012).

For a more detailed description of velocity models SC1_I and SC1_II and for the comparison with the anisotropic–ray–theory seismograms in these velocity models refer to Pšenčík, Farra & Tessmer (2012).

5.2. Measurement configuration

The synthetic seismograms generated by a vertical force are calculated at the receivers located in a vertical well at a distance of 1 km from the source. The source–receiver configuration in velocity models SC1_I and SC1_II is displayed in Figure 1.

The source time function is the Gabor signal $\cos(2\pi ft)\exp[-(2\pi ft/4)^2]$ with reference frequency $f = 50$ Hz, bandpass filtered by a cosine filter specified by frequencies 0 Hz, 5 Hz, 60 Hz and 100 Hz. The depths of the receivers are displayed in the plots of seismograms. The receivers record the following 3 components of displacement: radial component (along the line connecting the source and the top of the well, positive away from the source), transverse component (perpendicular to the source–receiver plane), and vertical component (positive downwards). The recording system is right–handed. For the prevailing–frequency approximation of the coupling ray theory, we naturally use prevailing frequency $f_0 = 50$ Hz.

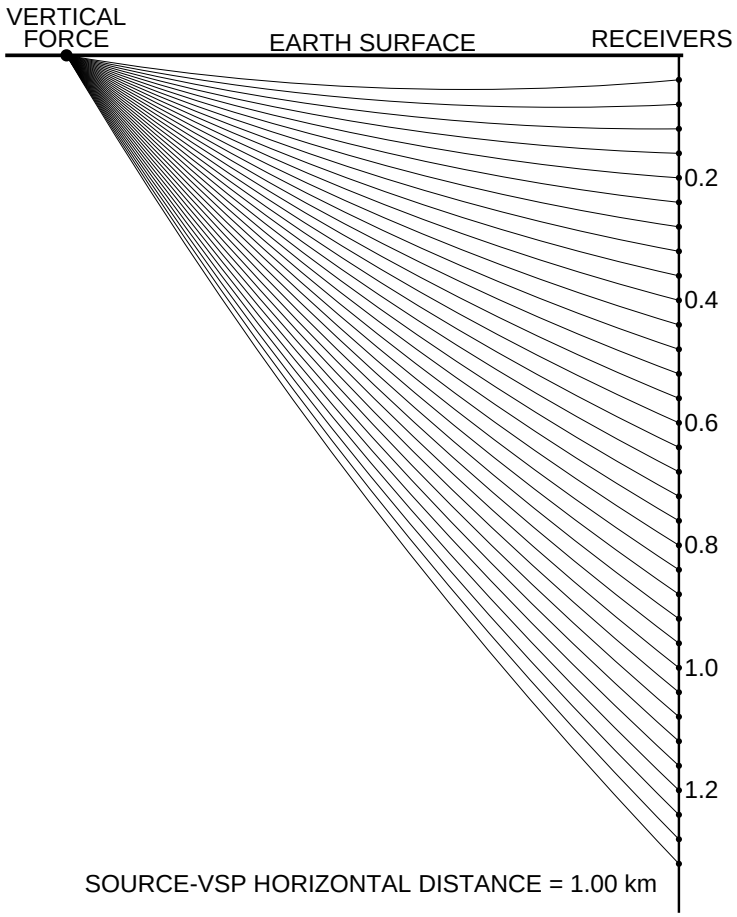

Figure 1: The source–receiver configuration for the calculation of synthetic seismograms, with a sketch of the reference rays. The source is located at the Earth's surface, the receivers are placed in the vertical well.

5.3. Comparison of synthetic seismograms

The synthetic seismograms in velocity models SC1_I and SC1_II are displayed in Figures 2–5. In both velocity models, we compare the prevailing–frequency approximation of the coupling ray theory along the anisotropic common S–wave reference rays with the Fourier pseudospectral method, and the prevailing–frequency approximation of the coupling ray theory along the SH and SV reference rays with the Fourier pseudospectral method. In each figure, the synthetic seismograms calculated by the prevailing–frequency approximation of the coupling ray theory and by the Fourier pseudospectral method are displayed in different colours. In each velocity model, the amplitude scaling is equal for all components and all receivers. Note that the second (transverse) component would vanish in the isotropic–ray–theory seismograms in these velocity models.

Along the anisotropic common S–wave reference rays, we use the quadratic perturbation expansions of travel times because they yield slightly more accurate synthetic seismograms than linear expansions. Along the SH and SV reference rays, we use the linear perturbation expansions of travel times. The presented numerical examples suggest that the linear perturbation expansions are sufficiently accurate in these velocity models. Since approximately transversely isotropic velocity models SC1_I and SC1_II display split intersection singularities, we applied the selection of arrivals based on polarization according to Klimeš & Bulant (2014a, sec. 4.1).

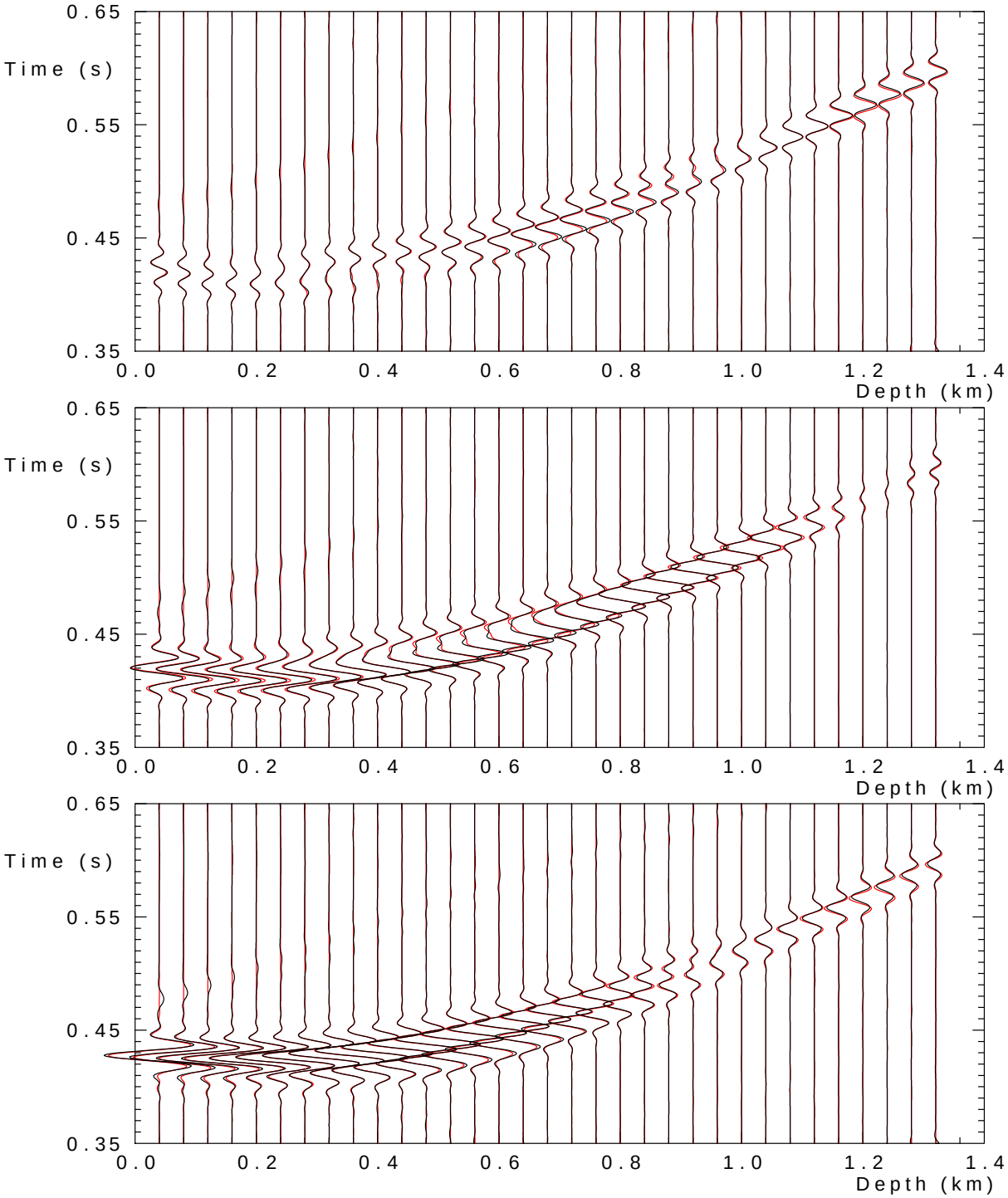

Figure 2: Radial, transverse and vertical component of the seismograms calculated in velocity model SC1_I. The **red** seismograms are calculated using the prevailing–frequency approximation of the coupling ray theory according to Klimeš & Bulant (2012) along the anisotropic common S–wave rays with the quadratic perturbation expansions of travel times. They are overlaid by the **black** seismograms calculated using the Fourier pseudospectral method by Pšenčík, Farra & Tessmer (2012) which is considered here as a nearly exact reference.

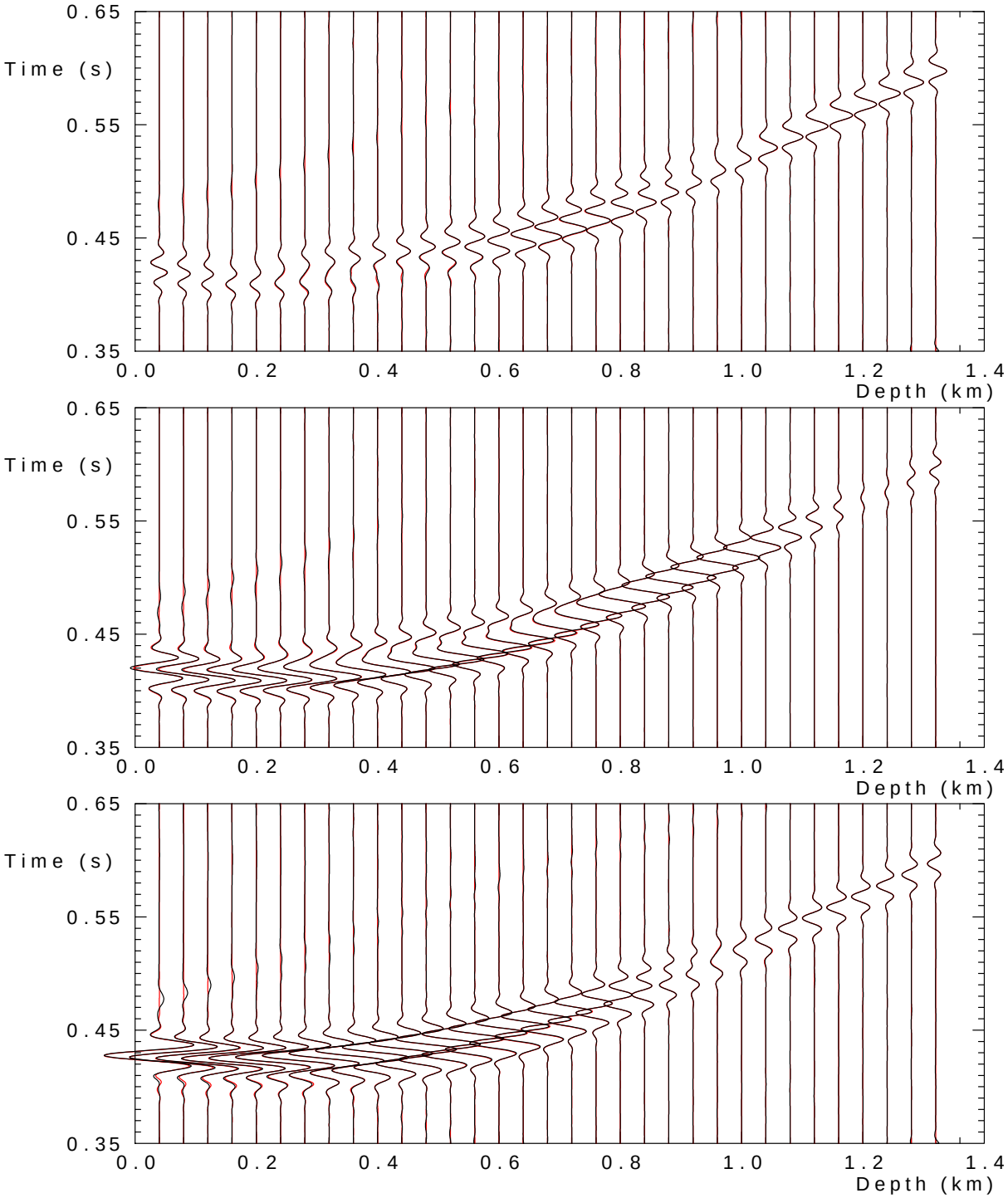

Figure 3: Radial, transverse and vertical component of the seismograms calculated in velocity model SC1_I. The **red** seismograms are calculated using the prevailing–frequency approximation of the coupling ray theory according to Klimeš & Bulant (2012) along the SH and SV reference rays traced according to this paper, with the linear perturbation expansions of travel times. They are overlaid by the **black** seismograms calculated using the Fourier pseudospectral method by Pšenčík, Farra & Tessmer (2012) which is considered here as a nearly exact reference. In comparison with Figure 2, the differences of the coupling ray theory from the Fourier pseudospectral method have obviously been reduced.

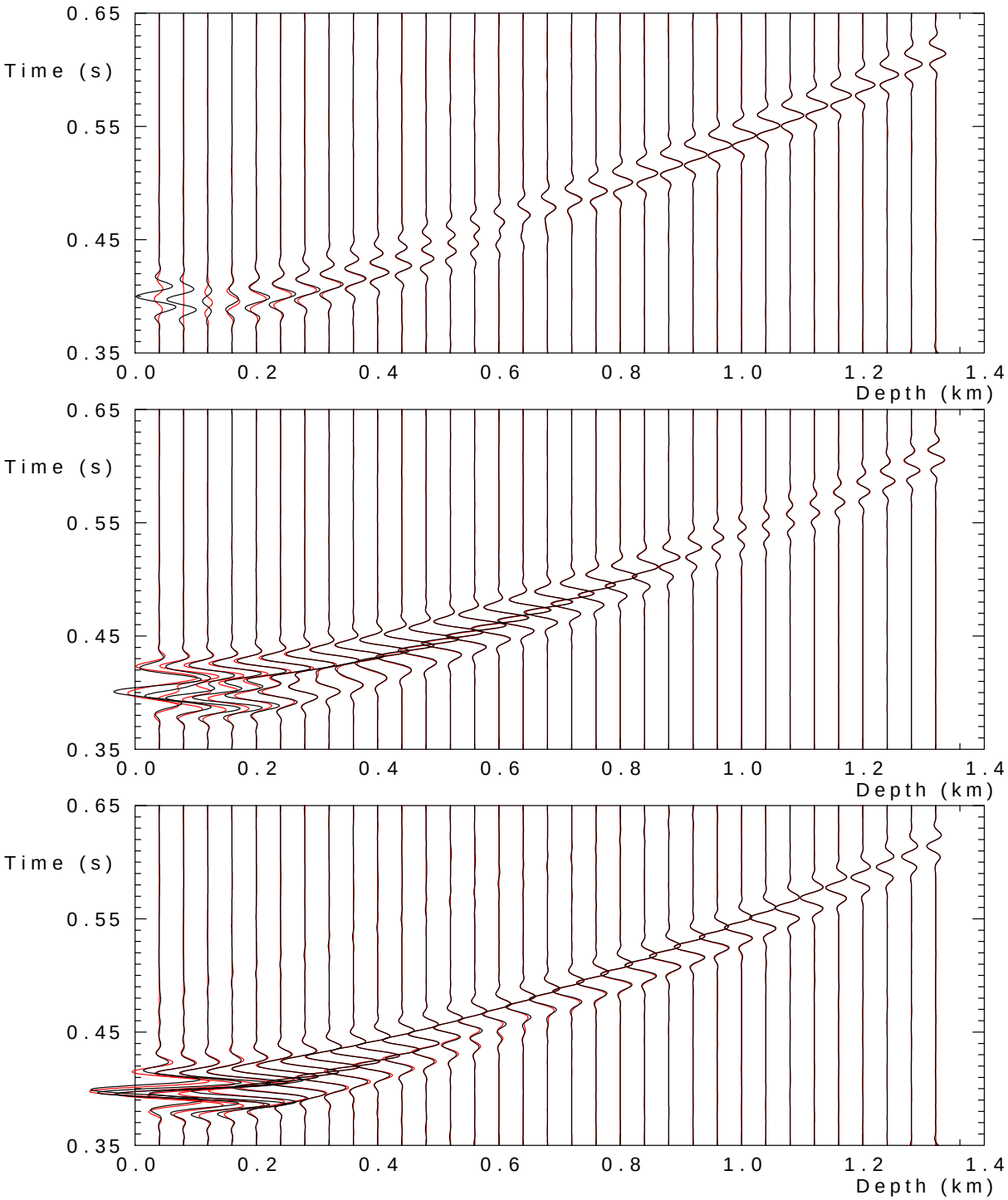

Figure 4: Radial, transverse and vertical component of the seismograms calculated in velocity model SC1_II. The **red** seismograms are calculated using the prevailing–frequency approximation of the coupling ray theory according to Klimeš & Bulant (2012) along the anisotropic common S–wave rays with the quadratic perturbation expansions of travel times. They are overlaid by the **black** seismograms calculated using the Fourier pseudospectral method by Pšenčík, Farra & Tessmer (2012) which is considered here as a nearly exact reference.

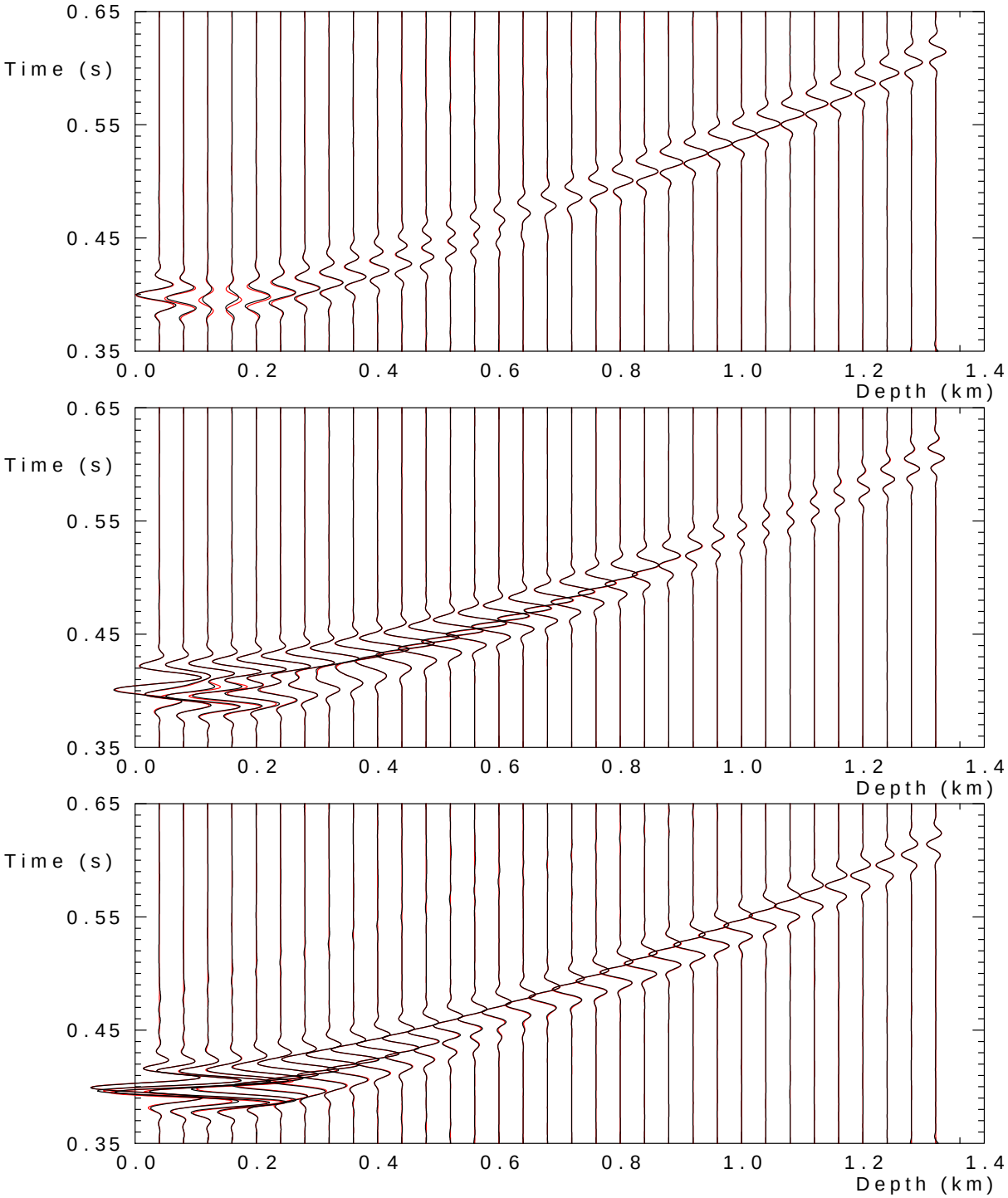

Figure 5: Radial, transverse and vertical component of the seismograms calculated in velocity model SC1_II. The **red** seismograms are calculated using the prevailing–frequency approximation of the coupling ray theory according to Klimeš & Bulant (2012) along the SH and SV reference rays traced according to this paper, with the linear perturbation expansions of travel times. They are overlaid by the **black** seismograms calculated using the Fourier pseudospectral method by Pšenčík, Farra & Tessmer (2012) which is considered here as a nearly exact reference. In comparison with Figure 4, the differences of the coupling ray theory from the Fourier pseudospectral method have considerably been reduced.

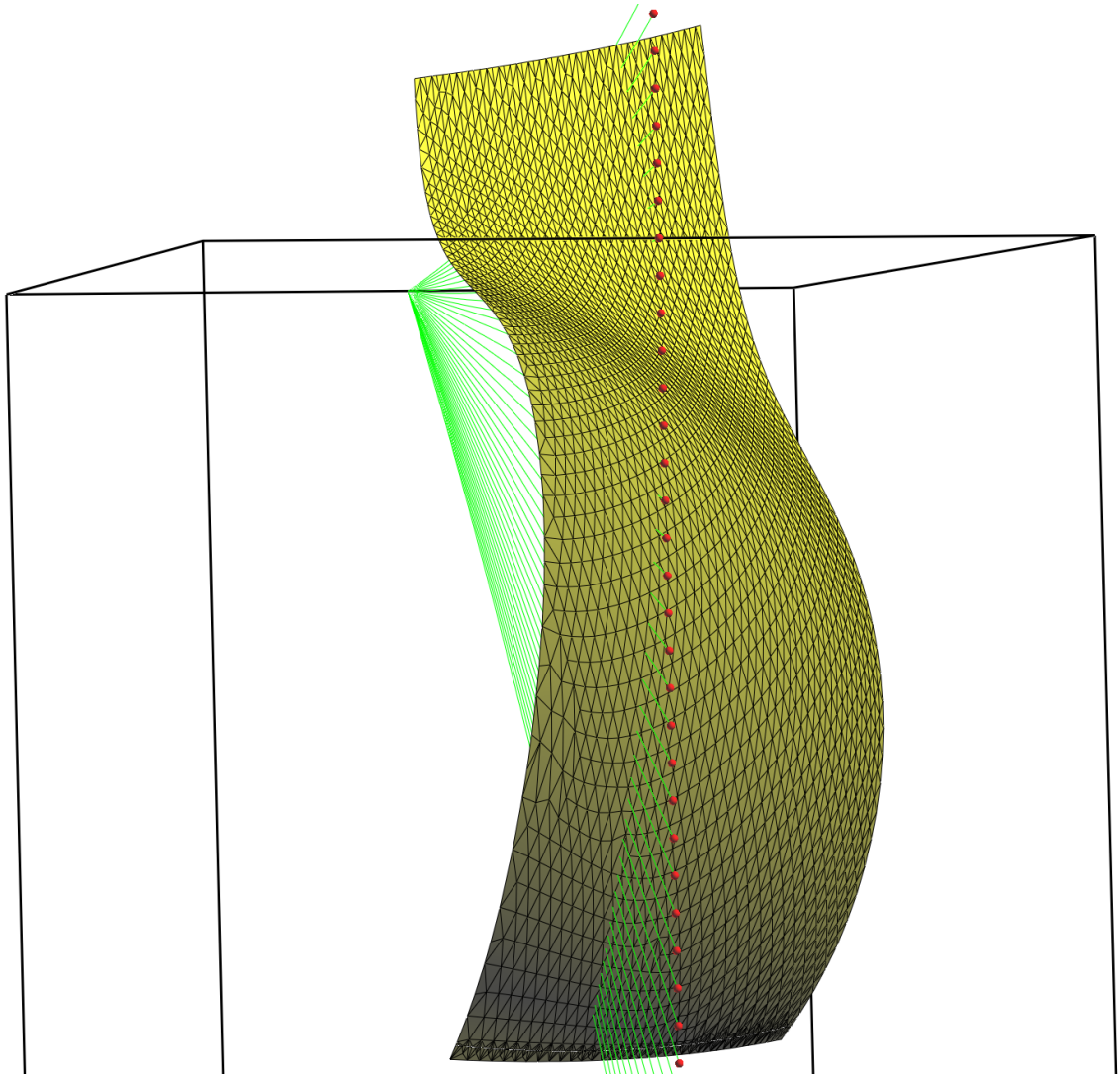

Figure 6: Two–point SV reference rays in velocity model SC1_II, together with a wavefront triangulated according to the ray tubes. The black lines are the edges of the computational volume. The surface (zero depth) corresponds to the top of the computational volume. The receivers are denoted by small red spheres. Only the receivers below the surface correspond to the receivers in the synthetic seismograms displayed in Figures 4 and 5. On the wavefront, we observe the belt of small geometrical spreading which intersects the receiver profile between the third and fourth receivers below the surface. Note that the wavefront looks like S curved, but it is just an optical illusion caused both by the curved sides of the displayed wavefront section and by varying triangular crossections of ray tubes, see Figure 7.

Whereas the coupling–ray–theory seismograms calculated along the anisotropic common S–wave reference rays in velocity model SC1_I (Figure 2) display small inaccuracies, the coupling–ray–theory seismograms calculated along the SH and SV reference rays (Figure 3) are nearly correct.

In velocity model SC1_II containing a split intersection singularity in the source–receiver plane, we observe a great inaccuracy of the coupling–ray–theory seismograms calculated along the anisotropic common S–wave reference rays (Figure 4). The coupling–ray–theory seismograms calculated along the SH and SV reference rays (Figure 5) represent a considerable accuracy improvement. However, some differences, mostly in amplitudes are still present. These differences are centred around the third and fourth

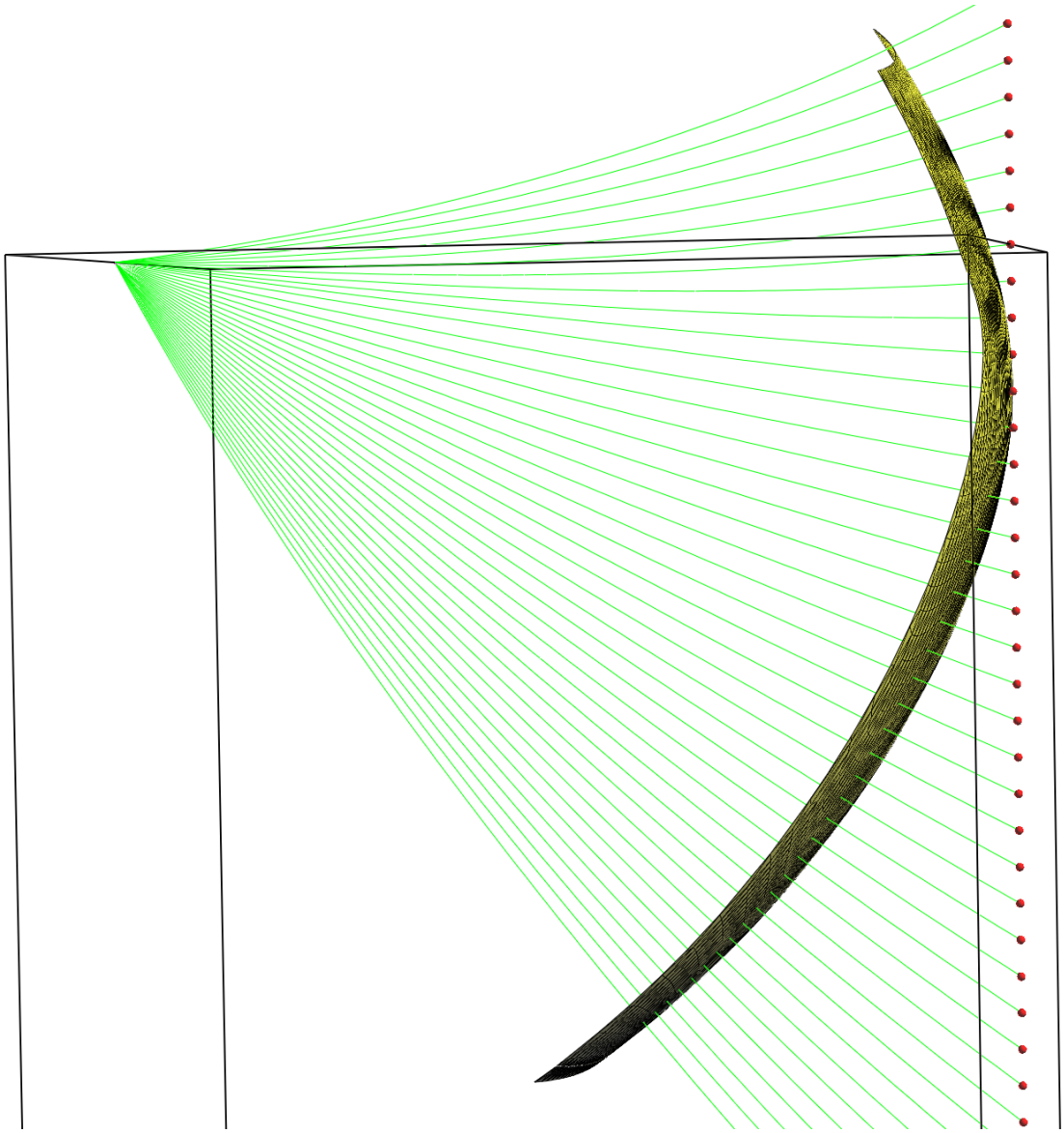

Figure 7: A side view of the wavefront section displayed in Figure 6. We see that the wavefront is convex with just moderate variation of its curvature.

receivers below the surface. We can also observe an increment of amplitudes of the faster S wave in this region. In this case, the faster S wave is the SV wave. We thus display the SV–wave wavefront tringulated according to the SV ray tubes in velocity model SC1_II in Figures 6 to 8. On the wavefront, we observe the belt of small geometrical spreading which intersects the receiver profile between the third and fourth receivers below the surface. This belt probably causes the increase of the zero–order ray–theory amplitudes in comparison with the correct amplitudes, similarly as in the vicinity of caustics. The resulting increase of the coupling–ray–theory amplitudes in comparison with the correct amplitudes in velocity model SC1_II may hopefully be corrected by the summation of the coupling–ray–theory Gaussian beams calculated along the SH and SV reference rays, which remains a challenge for our future research.

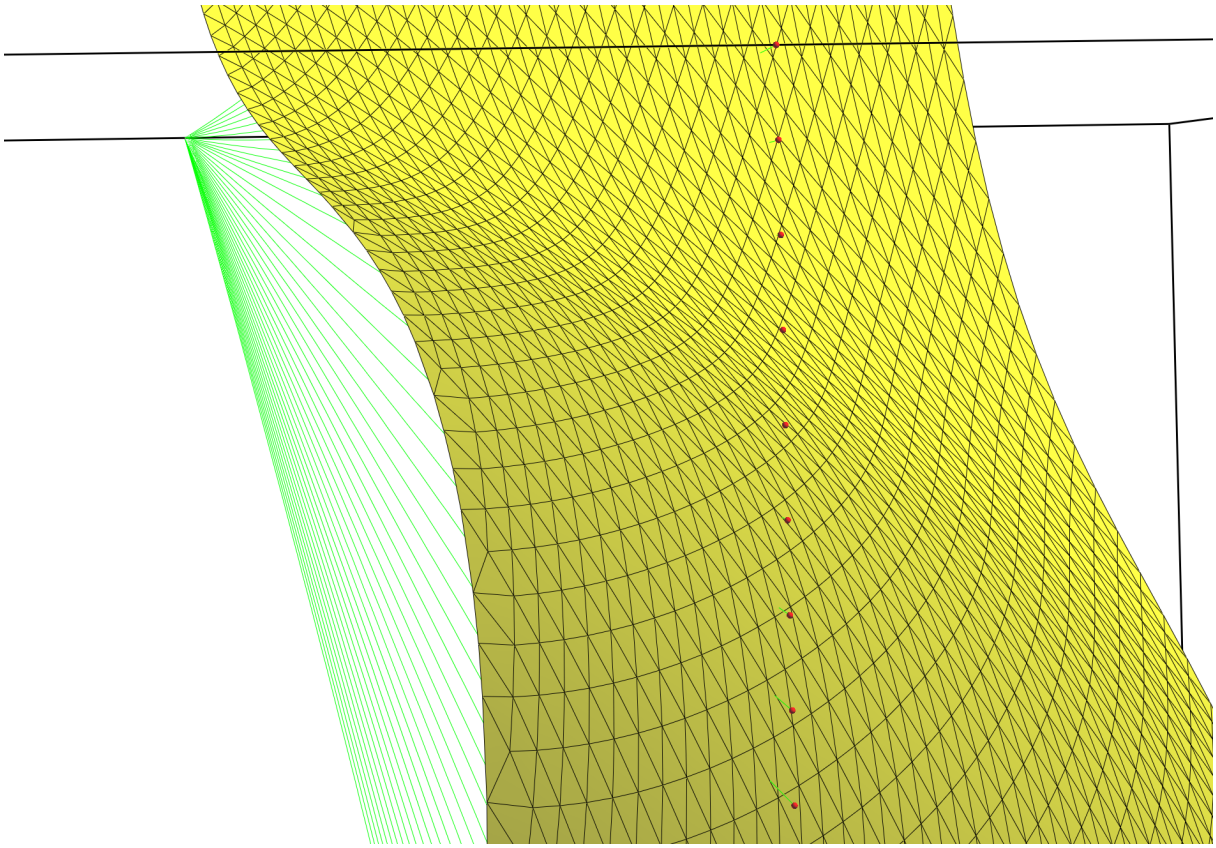

Figure 8: A detail of Figure 6, displaying the belt of small geometrical spreading which intersects the receiver profile between the third and fourth receivers below the surface. This belt probably causes the increase of the zero–order ray–theory amplitudes in comparison with the correct amplitudes, similarly as in the vicinity of caustics.

6. Conclusions

The SH and SV rays in transversely isotropic media or the SH and SV reference rays in approximately transversely isotropic media may represent very accurate reference rays for the coupling ray theory. To trace the SH and SV reference rays in an approximately transversely isotropic medium, we need the reference SH and SV Hamiltonian functions. The reference SH and SV Hamiltonian functions can be defined using the reference symmetry vector of an approximately transversely isotropic medium (Klimeš, 2015).

In this paper, we have proposed the expressions for the reference SH and SV Hamiltonian functions homogeneous of the second degree with respect to the slowness vector, and derived the expressions for their first–order and second–order phase–space derivatives, which are necessary for ray tracing and for the equations of geodesic deviation (dynamic ray tracing).

For the sake of simplicity, we assumed a constant reference symmetry vector of an approximately transversely isotropic medium in this paper. However, the presented equations can simply be generalized to generally heterogeneous dependence of the reference symmetry vector on the spatial coordinates using the equations by Klimeš (2015).

Improvement of the coupling–ray–theory synthetic seismograms calculated along the SH and SV reference rays in an approximately transversely isotropic medium have been demonstrated in velocity models QI2 and QI4 by Klimeš & Bulant (2014a), and in velocity models SC1_I and SC1_II in Section 5 of this paper.

Fixing the remaining inaccuracy of the zero–order ray–theory amplitudes in velocity model SC1_II using the summation of the coupling–ray–theory Gaussian beams calculated along the SH and SV reference rays remains a challenge for our future research.

Acknowledgements

We are grateful to Einar Iversen who encouraged us in this study. Ekkehart Tessmer kindly applied his Fourier pseudospectral method to calculating the seismograms which we used here as nearly exact reference seismograms.

The research has been supported by the Grant Agency of the Czech Republic under contract P210/10/0736, by the Ministry of Education of the Czech Republic within research projects MSM0021620860 and CzechGeo/EPOS LM2010008, and by the members of the consortium "Seismic Waves in Complex 3–D Structures" (see "http://sw3d.cz").

References

Bakker, P.M. (2002): Coupled anisotropic shear wave raytracing in situations where associated slowness sheets are almost tangent. *Pure appl. Geophys.*, **159**, 1403–1417.

Bucha, V. & Bulant, P. (eds.) (2015): SW3D–CD–19 (DVD–ROM). *Seismic Waves in Complex 3–D Structures*, **25**, 209–210, online at "http://sw3d.cz".

Bulant, P. & Klimeš, L. (2002): Numerical algorithm of the coupling ray theory in weakly anisotropic media. *Pure appl. Geophys.*, **159**, 1419–1435.

Bulant, P. & Klimeš, L. (2008): Numerical comparison of the isotropic–common–ray and anisotropic–common–ray approximations of the coupling ray theory. *Geophys. J. int.*, **175**, 357–374.

Bulant, P. & Klimeš, L. (2014): Anisotropic–ray–theory geodesic deviation and two–point ray tracing through a split intersection singularity. *Seismic Waves in Complex 3–D Structures*, **24**, 179–187, online at "http://sw3d.cz".

Bulant, P., Pšenčík, I., Farra, V. & Tessmer, E. (2011): Comparison of the anisotropic–common–ray approximation of the coupling ray theory for S waves with the Fourier pseudo-spectral method in weakly anisotropic models. *Seismic Waves in Complex 3–D Structures*, **21**, 167–183, online at "http://sw3d.cz".

Chapman, C.H. & Shearer, P.M. (1989): Ray tracing in azimuthally anisotropic media — II. Quasi–shear wave coupling. *Geophys. J.*, **96**, 65–83.

Crampin, S. (1981): A review of wave motion in anisotropic and cracked elastic–media. *Wave Motion*, **3**, 343–391.

Klimeš, L. (2006): Common–ray tracing and dynamic ray tracing for S waves in a smooth elastic anisotropic medium. *Stud. geophys. geod.*, **50**, 449–461.

Klimeš, L. (2015): Determination of the reference symmetry axis of a generally anisotropic medium which is approximately transversely isotropic. *Seismic Waves in Complex 3–D Structures*, **25**, 177–185, online at "http://sw3d.cz".

Klimeš, L. & Bulant, P. (2004): Errors due to the common ray approximations of the coupling ray theory. *Stud. geophys. geod.*, **48**, 117–142.

Klimeš, L. & Bulant, P. (2006): Errors due to the anisotropic–common–ray approximation of the coupling ray theory. *Stud. geophys. geod.*, **50**, 463–477.

Klimeš, L. & Bulant, P. (2012): Single–frequency approximation of the coupling ray theory. *Seismic Waves in Complex 3–D Structures*, **22**, 143–167, online at "http://sw3d.cz".

Klimeš, L. & Bulant, P. (2014a): Prevailing–frequency approximation of the coupling ray theory for S waves along the SH and SV reference rays in a transversely isotropic medium. *Seismic Waves in Complex 3–D Structures*, **24**, 165–177, online at "http://sw3d.cz".

Klimeš, L. & Bulant, P. (2014b): Anisotropic–ray–theory rays in velocity model SC1_II with a split intersection singularity. *Seismic Waves in Complex 3–D Structures*, **24**, 189–205, online at "http://sw3d.cz".

Pšenčík, I., Farra, V. & Tessmer, E. (2012): Comparison of the FORT approximation of the coupling ray theory with the Fourier pseudospectral method. *Stud. geophys. geod.*, **56**, 35–64.